The fcc - bcc structural transition: I. A band theoretical study for Li, K, Rb, Ca, Sr, and the transition metals Ti and V

1996 J. Phys.: Condens. Matter 8 799

(http://iopscience.iop.org/0953-8984/8/7/006)

J. Phys.: Condens. Matter **8** (1996) 799–815. Printed in the UK

The fcc–bcc structural transition: I. A band theoretical study for Li, K, Rb, Ca, Sr, and the transition metals Ti and V

V L Sliwko, P Mohn, K Schwarz and P Blaha

Technical University of Vienna, Getreidemarkt 9/158, A-1060 Vienna, Austria

Received 24 August 1995

Abstract. Employing a high-precision band structure method (FP LAPW—full potential linearized augmented plane wave) we calculate the total energy variation along the tetragonal distortion path connecting the body centred cubic (bcc) and the face centred cubic (fcc) structures. The total energy along this Bain transformation is calculated, varying c/a and volume, providing a first-principles energy surface which has two minima as a function of c/a. These are shallow and occur for the sp metals at the two cubic structures, while Ti (V) has a minimum at fcc (bcc) but a saddle point (i.e. a minimum in volume and a maximum with respect to c/a) at the other cubic structure. These features can be analysed in terms of an interplay between the Madelung contribution and the band energies. Our total energy results allow us to calculate the elastic constants C_{11} and C_{12} and to study the influence of pressure on the phase stability. These energy surfaces will be used in part II of this paper to investigate finite-temperature effects by mapping them to a Landau–Ginzburg expansion.

1. Introduction

Martensitic phase transitions (MPTs) have interested scientists for more than a century leading to an enormous amount of literature, which we do not attempt to summarize here, but we notice that many open questions remain. Although metallurgists have developed a large number of technologically important applications (e.g. shape memory alloys) and know well how to make use of MPTs, the theoretical and fundamental understanding of this phenomenon is still far from being complete. In contrast to diffusive phase transitions an MPT is a collective phenomenon where a crystal undergoes a first-order transition from an austenitic (high-temperature) modification to a martensitic (low-temperature) structure with a hysteretic behaviour typical for this phase transition. The width of the hysteresis ΔT, the discontinuity in the specific heat at constant pressure ΔC_p, and the volume change $\Delta V/V$ are found to be characteristic quantities to distinguish between various types of martensite. Around the MPT one usually observes a softening of some elastic constants together with a large elastic anisotropy. In some systems martensitic precursor effects appear as local distortions leading to the well known 'tweed structures'.

The development of theoretical models for the MPT was pioneered by Cochran [1] and Anderson [2] who independently formulated the soft-mode model according to which the effective frequency of one phonon branch becomes zero at a temperature T_0, triggering the phase transition, but only very few systems show this behaviour [3, 4]. Krumhansl and Gooding [5] proposed a model based on anharmonicities in the order parameter (see part II

0953-8984/96/070799+17$19.50

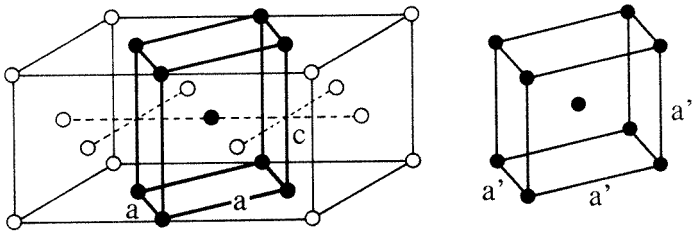

Figure 1. A representation of the fcc and bcc lattices assuming a bct (body centred tetragonal) cell which allows a continuous (Bain) transformation between them.

[6] of this paper) while Vul and Harmon [7] discussed a fluctuationless mechanism where the MPT is triggered by defects in the crystal structure. A fairly complete overview on martensitic phenomena can be found in [8].

If a crystal undergoes a transition from one structure into another, individual atoms in the unit cell or complete atomic planes in the whole crystal must move to new positions in an orderly fashion. Out of the multitude of possible geometries for such a transition between the body centred cubic (bcc) and the face centred cubic (fcc) crystal structure the Bain transformation is by far the simplest. It has been known since 1924 when E C Bain [9] described the MPT by a continuous displacement of one or more atoms per unit cell. From his work on quenched steel he found an orientational relationship between the austenitic and the martensitic phase, namely that the [001] plane of both the bcc and fcc structure remains unchanged during the transition. Bain described this transition between the bcc and fcc structure via a tetragonal distortion shown in figure 1. Both the fcc and bcc lattice can be described as special case of a body centred tetragonal (bct) unit cell. In the fcc case a and b are equal and the lattice vector c has the length $a\sqrt{2}$ while in the bcc case all three lattice vectors have equal length a'. The Bain transformation between the fcc and the bcc lattice is thus described by the continuous change of a single variable, namely the c/a ratio, so that $c/a = \sqrt{2}$ refers to the fcc and $c/a = 1$ to the bcc structure. It should be noted that this Bain transformation is just one of 24 possible paths (given the existence of a habit plane) between these two structures and that other, usually more complicated, transformations can occur and have been found experimentally.

We have made a systematic investigation of the fcc $\leftrightarrow$ bcc transition along the Bain path which is sufficiently simple to make computations feasible but should lead to a basic understanding of MPT. This study is undertaken for the simple metals Li, K, Rb, Ca and Sr and for the early transition elements Ti and V. In our study of the alkalines we omitted Na, since already several theoretical investigations are available (see e.g. [10], [11] and references therein). In this paper we describe the band structure results which are valid at $T = 0$ K but can be mapped to a Landau expansion and thus provide a basis for a finite-temperature (mean field) study which is contained in part II [6].

2. Computational details

We use quantum mechanical calculations to obtain the total energy at $T = 0$ on a first-principles basis. We compute the electronic band structure within the density functional theory and the local density approximation (LDA) by means of the full-potential linearized-augmented-plane-wave (FP LAPW) method employing the WIEN95 code developed by Blaha *et al* [12]. Exchange and correlation effects are treated by LDA using the

parametrization by Hedin and Lundqvist [13]. It will be shown below that for some systems the energy differences are only fractions of 1 mRyd, and therefore the calculations were carried out for a sufficiently large number of $\boldsymbol{k}$-points in the irreducible wedge of the bct Brillouin zone (between 540 and 1800 $\boldsymbol{k}$-points, depending on the system). A $\boldsymbol{k}$-grid that is about uniform for $c/a = 1.2$ was kept fixed throughout the calculations in order to avoid discontinuities in the total energy that could be caused if the number of grid points were changed discontinuously as a function of cell dimensions. Furthermore very high precision in the total energy results is necessary and was achieved by using a plane-wave cut-off $RK_{\max} = 9$ (for definitions see [12]) leading to about 140 (plane-wave) basis functions. Inside the atomic spheres the potential and charge density are expanded in crystal harmonics up to $L = 6$; in the interstitial region a Fourier series with 150 stars of $\boldsymbol{K}$ is used. In each self-consistency cycle the core states are treated fully relativistically and the Hamiltonian for the valence (and semicore) states is calculated in a scalar relativistic version (without spin–orbit corrections). The total energy (at $T = 0$) is computed as a function of volume V and c/a (Bain variable), the two most important parameters. For each of the seven systems we performed calculations for about eight different volumes and 10 different c/a ratios. From this series of self-consistent FP LAPW calculations we derive total energy surfaces $E(V, c/a)$ in the volume–Bain variable space. In contrast to earlier investigations [10, 14] which concentrated on the c/a variation of the total energy, we included the volume as another crucial parameter for the thermodynamic phase stability. It will be shown (subsection 3.4) that the volume change calculated at $T = 0$ K can be related to the slope in the P, T phase diagram. We would like to mention that this part of our work is similar to previous investigations by Chen *et al* [15] for the hcp $\leftrightarrow$ bcc transition in barium and the reader should be aware that other quantum mechanical models have been applied to this problem by various authors [14–17].

By fitting the FP LAPW total energies to a polynomial, we obtain an analytic expression for the energy surface $E(c/a, V)$ given by

$$E(c/a, V) = \sum_{i=0,n} \sum_{j=0,m} A_{ij} (c/a)^i V^j. \tag{1}$$

To monitor the convergence of the fit we performed a least-squares procedure using orthogonal Chebychev polynomials from which the polynomial acc. to (1) was derived. The fit coefficients A_{ij} for all metals studied are given in the appendix.

The analytic expression for the total energy (1) allows us to calculate several characteristic quantities such as the bulk modulus

$$B = V \partial^2 E(c/a, V)/\partial V^2 = \big(C_{11} + 2C_{12}\big)/3 \qquad c/a \text{ constant} \tag{2}$$

or the tetragonal shear constant

$$C' = (1/V)\partial^2 E(c/a, V)/\partial (c/a)^2 = \big(C_{11} + C_{12}\big)/2 \qquad V \text{ constant.} \tag{3}$$

The definitions of the elastic constants C_{11} and C_{12} are self-evident and it is straightforward to calculate the equilibrium values of volume V and Bain variable c/a. Formally the expansion given in (1) is equivalent to the one for the soft-mode model proposed by Clapp [3] who explains the occurrence of MPTs by nucleation due to local strains.

3. Total energy surfaces as a function of c/a and V

In the following section we present the result of our band structure calculations and show for each system investigated the total energy surface. In the present study we find either

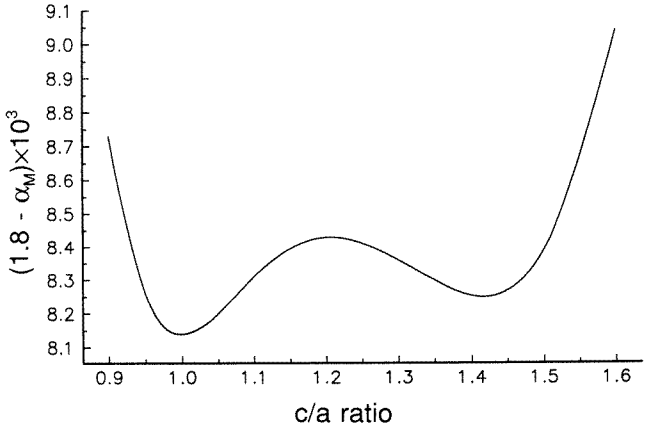

Figure 2. Madelung constant α_M as a function of c/a for a bct lattice.

fcc or bcc as the most stable modification which is associated with a local energy minimum with respect to V and c/a. However, this does not need to be the absolute minimum, since other phases, which might lead to an even lower total energy, are not investigated. At first it seems surprising that (for each volume) the energy appears to be an extremum (either minimum or maximum) at the 'cubic' values of c/a (i.e. $c/a = 1$ for bcc, $c/a = \sqrt{2}$ for fcc). This extremal condition is in fact a general feature of cubic systems and can be derived from the elastic energy assuming the volume remains constant [18]. Therefore this observation suggests that the lattice geometry plays an important role. If one varies the c/a ratio for a tetragonal unit cell as shown in figure 1 the number of next-nearest neighbours becomes a relative maximum for $c/a = 1$ (bcc; 8 n.n.) and an absolute maximum for $c/a = \sqrt{2}$ (fcc; 12 n.n.) while for all other values of c/a the number of n.n. is below eight.

It has been shown that the total energy can be decomposed into terms which depend only on volume, and two contributions, namely the band energy (the sum over the occupied states) and the electrostatic Ewald energy, which depend on the c/a ratio [19]. Therefore the latter two terms govern the total energy for constant volume. The electrostatic Ewald energy E_{Ew} is given by

$$E_{Ew} = \left(1.8 - \alpha_M\right)\left(q^2/\Omega_{MT}^2\right)\Omega_{WS}^2/R_{WS} \tag{4}$$

where Ω_{WS} and Ω_{MT} are the volume of the Wigner–Seitz and the muffin-tin sphere, respectively; R_{WS} is the Wigner–Seitz radius and q is the charge inside the Wigner–Seitz sphere (equal to the nuclear charge for monoatomic systems) minus the charge inside the (smaller) non-overlapping muffin-tin sphere. For metallic systems the variation of E_{Ew} along the Bain path is governed by the c/a dependence of α_M, since Ω_{WS}^2/R_{WS} is constant for fixed volume and q/Ω_{MT} is nearly constant for slowly varying electron densities. In fact for vanadium even q varies little, between 1.432 and 1.462 electrons in the range of $0.8 < c/a < 1.6$.

The function $\alpha_M(c/a)$ shows (figure 2) a double-well structure with two minima, one at $c/a = 1$ (bcc) and the other at $\sqrt{2}$ (fcc). This behaviour is due to the self-reciprocity of the bcc and fcc structure as discussed in the earlier literature [20]. For $c/a < 0.9$ and $c/a > 1.7$, the Ewald energy rises sharply, since electrostatics makes such highly distorted bct lattices very unfavourable. It should be noted, however, that in ionic systems, where q is no longer nearly constant, E_{Ew} can (in contrast to metals) deviate substantially from the

double-well behaviour of α_M. For example, it has been shown [21] that in CsI the pressure induced tetragonal distortion is due to the electrostatic contribution to the total energy.

The band energy (sum over all occupied states) can (to a good approximation) be reduced to the contribution from the valence electrons, since the core energies do not change for constant volume. The band energy is given by

$$E_B = \int_{\varepsilon_0}^{\varepsilon_F} \varepsilon N(\varepsilon)\,\mathrm{d}\varepsilon \tag{5}$$

where ε_0 denotes the bottom of the valence band, ε_F is the Fermi energy, and $N(\varepsilon)$ is the density of states of the valence electrons. For our metallic systems E_B contains the essential information on bonding and thus determines the equilibrium geometry of the lattice. This energy decomposition will be used (subsection 3.8) to analyze the total energy of titanium and vanadium.

Below we present the $T = 0$ K results of our band structure calculations for each system and discuss the related properties. For some cases we decompose the total energy into E_{Ew} and E_B in order to illustrate the well known different bonding mechanism for simple (sp-band systems) and transition metals (d-band systems). Unless stated differently our results are compared to the experimental phase diagrams taken from the book by Young [22].

3.1. Lithium

The total energy surface of Li (figure 3) shows that at the equilibrium volume the close-packed (fcc) structure is favoured over the bcc modification, although for the latter a local minimum occurs at $c/a = 1$. Experimentally the structure at $T = 0$ is found to be close packed, but in a hexagonal polytype (hcp or 9R [23]). It was confirmed by a previous investigation [24] using the same band structure code [12] that the hcp structure (with a c/a ratio slightly deviating from the ideal value of $\sqrt{(8/3)}$) is even more stable than the fcc. At the equilibrium volume the energy difference between the bcc and the fcc structure is about 0.16 mRyd. Under external pressure P this energy difference is increased in favour of the fcc structure (figure 4). The experimental phase diagram also shows that the stability range of the fcc structure is increased under pressure, which means that the critical temperature for the phase transition from fcc to bcc increases too ($\mathrm{d}p/\mathrm{d}T$ is positive). This observation implies that the temperature at which the MPT appears is related to the $T = 0$ K energy difference between the martensitic and the austenitic phase. A careful examination of the $E(c/a)$ curves (figure 4) shows that the metastable minimum at $c/a = 1$ (for $P = 0$) shifts under pressure to smaller values of c/a and a local maximum appears at $c/a = 1$. For Li this feature occurs only under pressure but it is common for the transition metal systems (see subsection 3.8). This observation implies that under pressure the 2p states are lowered in energy and thus form s,p hybrid bands which favour directional bonds comparable to the early transition metals investigated. From this analogy between Li and the transition metals, and the fact that this behaviour is not found for the heavier alkaline metals, where the energy difference between the s and p states is too large for an effective hybridization, we conclude that the formation of directional bonds is responsible for the local minimum at a c/a ratio smaller than unity.

It should be noted that earlier band structure investigations based on the ASA (atomic sphere approximation) assuming a spherically symmetric potential, e.g. within the LMTO (linear muffin-tin orbital) method, found the bcc structure as ground state [25, 26], while FP LAPW calculations [27] predict fcc lower than bcc and find hcp as the ground state [24] in

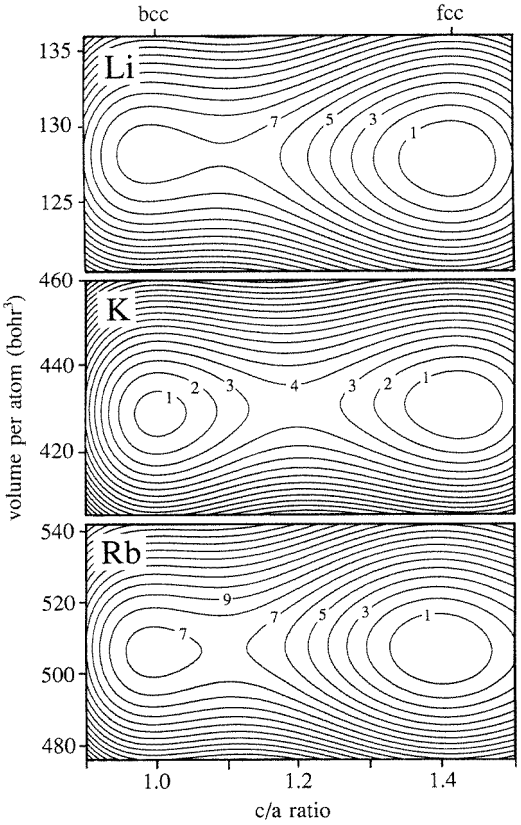

Figure 3. Total energy contours of Li, K, and Rb as a function of c/a and volume per atom. The labels on the contour lines are in multiples of 0.025 mRyd.

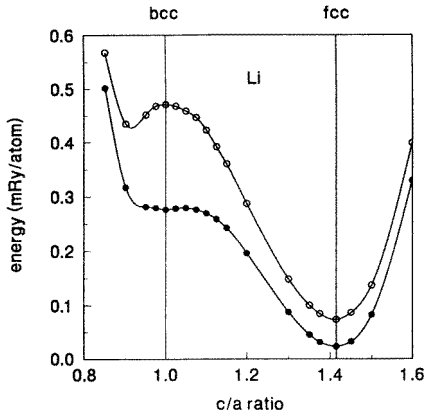

Figure 4. The energy variation of Li as a function of c/a for the equilibrium volume (108 bohr^3; full circles) and under pressure of 2 GPa ($V = 95$ bohr^3; open circles). The two curves are shifted arbitrarily.

agreement with pseudopotential calculations (without the ASA [28, 29]).

3.2. Potassium

The energy surface of K (figure 3) shows two minima at $c/a = 1$ and $c/a = \sqrt{2}$ with the fcc structure being slightly more stable by about 0.02 mRyd. This result has also been obtained by an independent APW [11] and a high-precision FP LAPW calculation [30], while other theoretical investigations [26, 29, 31] obtained a bcc ground state. The experimental situation is not completely clear but there is some evidence for a lattice distortion at low temperature [32, 33] and there are indications that the fcc structure becomes more stable under pressure.

3.3. Rubidium

We find fcc as ground state (figure 3) and a very shallow minimum at $c/a = 1$ which is about 0.17 mRyd above the fcc modification. Experimentally Rb is bcc at room temperature and there is a pressure induced phase transition to the fcc structure. The low-temperature phase diagram has not yet been completely resolved but there is again evidence for an instability of the bcc phase at low temperature [34]. This result is supported by the slope of the bcc/fcc phase boundary in the P, T diagram. Our calculation shows that under pressure the fcc modification becomes progressively more stable with respect to the bcc structure (a similar behaviour as in Li) and this is in agreement with the phase diagram, according to which for pressures larger than ≈9 GPa the fcc structure is stable up to the melting temperature. In contrast to our result, an *ab initio* pseudopotential investigation [35] found bcc more stable than fcc and a transition to fcc at about 5.2 GPa. The very low value of the shear constant C' (table 1), the lowest of the whole periodic table, makes the Rb lattice very unstable against a tetragonal distortion.

Table 1. Calculated and experimental (in brackets) elastic data for Li, K, and Rb. A comparison with experiment is only possible for the low-temperature structure; experimental data are taken from [49] for the structure specified. The volume is given as volume per atom.

	B (GPa)	C' (GPa)	C_{11} (GPa)	C_{12} (GPa)	V_{equil} (bohr^3)
Li fcc	15.2 (12.0)	1.3 (1.1)	16.9 (13.4)	14.3 (11.2)	127.7 (141.8)
Li bcc	15.4	1.2	17	14.7	128.1
K fcc	5.2	0.4	5.7	5.0	430.4
K bcc	5.4 (3.4)	0.6 (0.3)	6.1 (3.7)	4.9 (3.2)	428.7 (481.8)
Rb fcc	4.2	0.3	4.6	4.0	518.9
Rb bcc	4.1 (2.6)	0.3 (0.3)	4.5 (3.0)	3.8 (2.4)	519.6 (588.4)

3.4. Alkaline metals

According to our calculations all three simple metals Li, K and Rb behave similarly since at zero pressure the fcc structure is more stable than the bcc modification. The elastic constants are given in table 1. Since the total energy of these three metals has two minima (a stable and a metastable one) we calculate B, C', C_{11} and C_{12} for both cubic structures. A comparison with experiment, however, can only be made for the stable (low-temperature) phase. Table 1 demonstrates that all equilibrium quantities are in fair agreement with experiment. The bulk modulus is systematically overestimated and the equilibrium volume is about 10–15% smaller than experiment, deviations typical within LDA calculations.

Although it has been shown for Na [36] that for small changes in volume the barrier height separating the two phases remains fairly constant, this picture alters for larger

pressure. The fcc stability increases for Li and Rb, while for K the opposite behaviour is found. In the former case there is a positive slope of the phase boundary in the P, T phase diagram between the low-temperature (fcc) and the high-temperature (bcc) phase but in the latter case (of K) the fcc phase becomes less stable under pressure and the slope of the phase boundary is negative. This effect can be understood from Gibbs' phase rule for a one-component system, where the Clausius–Clapeyron equation defines the slope of the phase boundary:

$$\mathrm{d}P_T/\mathrm{d}T = \Delta S/\Delta V = \big(S_{bcc} - S_{fcc}\big)\big/\big(V_{bcc} - V_{fcc}\big). \tag{6}$$

In an entropy driven phase transition the entropy of the high-temperature phase (here S_{bcc}) must be larger than that of the lower-temperature phase (here S_{fcc}) in order to lower the free energy at high temperatures. Therefore in the present case ΔS must be positive and consequently the volume difference determines the sign of the slope [37]. By taking the respective values from table 1 we find $\mathrm{d}P_T/\mathrm{d}T$ to be positive for Li and Rb but negative for K, in complete agreement with the experimental phase diagrams. It should be noted that this analysis holds for Na too (table 3 of [11]) where LAPW calculations predict a negative ΔV leading to a negative $\mathrm{d}P_T/\mathrm{d}T$ in accord with experiment.

These macroscopic (thermodynamic) results discussed above must have a microscopic origin. When one compares the electronic band structure of the four alkaline metals [11] one notices that for Li and Rb the Fermi energy ε_F is located in a peak of the density of states caused by a flat band at the surface of the first Brillouin zone, but this is not the case for K and Na. According to Jones [38] a structural instability occurs if the Fermi surface touches the Brillouin zone. Under pressure, the band width is increased and states which were unoccupied at the equilibrium volume are lowered in energy and thus become occupied, leading to a lowering of ε_F, and consequently ε_F moves away from the 'unstable' peak position, increasing the fcc stability.

3.5. Calcium

Ca is a group II element and its ground state is fcc. Our calculation correctly predicts this ground state (figure 5) but shows a very shallow minimum at $c/a = 1$. At a pressure of about 19.5 GPa there is a transition into the bcc structure [39] which has been reproduced by Wentzcovitch and Krakauer using FP LAPW calculations [17]. They studied an interesting alternative path with respect to the Bain transformation and assumed a mechanism derived from Burgers' suggestion [40] for the hcp $\leftrightarrow$ bcc transformation. Since there exists a simple (but approximate) geometrical relationship between Bain's and Burgers' transformations, it is not surprising that the two paths hardly differ in total energy. In figure 6 we show the c/a dependence of the total energy at different volumes (pressures). It can be clearly seen that the fcc minimum disappears and (at $V_T \approx 150$ au) the system undergoes a pressure induced discontinuous phase transition to the bcc structure. Our results are in agreement with both the calculations mentioned above [17] and the experimental results cited therein. The slope of the phase boundary derived from (6) agrees in sign with experiment.

The critical pressure found for the fcc $\leftrightarrow$ bcc transition is about 20 GPa and is calculated directly from the total energy surface. It should however be noted that the critical pressure for the phase transition can no longer be calculated from the volumes V_{eq} and V_T and the fcc bulk modulus B, since the harmonic approximation assumed in the calculation of B no longer holds for a volume ratio $V_T/V_{eq} \approx 0.6$.

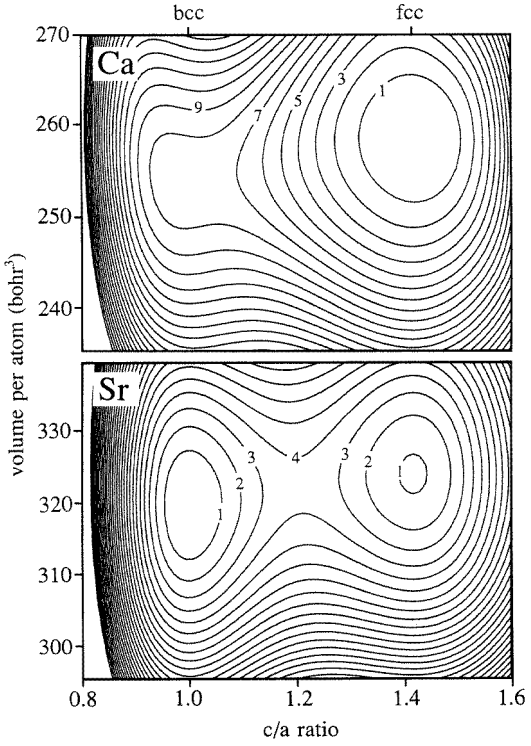

Figure 5. Total energy contours of Ca and Sr as a function of c/a and volume per atom. The labels on the contour lines are in multiples of 0.1 mRyd.

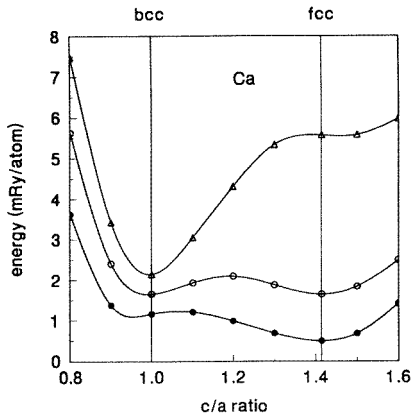

Figure 6. The energy variation of Ca as a function of c/a for three volumes: $V_{eq} = 256.9$ bohr^3 (full circles), $V = 210$ bohr^3 (open circles), and $V = 150$ bohr^3 (triangles). The three curves are shifted arbitrarily.

3.6. Strontium

According to the available experimental data, our calculation incorrectly predicts bcc as ground state (figure 5) but the energy difference between the bcc and fcc modification is

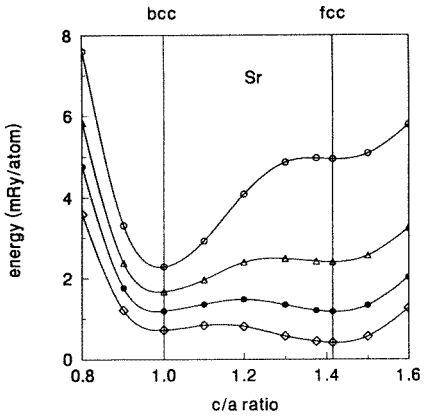

Figure 7. The energy variation of Sr as a function of c/a for volumes: $V_{eq} = 324$ bohr^3 (full circles), $V = 360$ bohr^3 (diamonds), $V = 290$ bohr^3 (triangles), and $V = 210$ bohr^3 (open circles). The four curves are shifted arbitrarily.

below 0.05 mRyd (<7.5 K) in favour of bcc. We even tried to improve the basis set of our band structure calculation and performed additional band calculations for Sr where we treated the low-lying 3p (semicore) states by local orbitals [41], a procedure that guarantees a proper orthogonalization of the valence states to the lower-lying semicore states. However, this new set of calculations did not change the original result. Experimentally the ground state at room temperature is found to be fcc but the bcc structure must be very close since already 3.5 GPa are enough to drive Sr to the bcc phase. If we assume that our fcc minimum would be the ground state, we find a pressure induced transition to the bcc state at about 4 GPa (figure 7), which means that regardless of the actual ground state (bcc or fcc) the energy barrier is described properly. Earlier LMTO calculations gave essentially the same results [42].

3.7. Summary of the simple metal results

The equilibrium data for Ca and Sr are summarized in table 2 which shows that our results are as close to experimental values as one can expect within the LDA. All five simple metals investigated have the same characteristic double-well structure where both bcc and fcc modifications are found to be at a (relative) minimum of the total energy. The mutual stabilization energies are small, which suggests that the major contribution to the stability stems from the electrostatic Ewald energy E_{Ew} as discussed above. A decomposition of the total energy into E_{Ew} and the band energy E_B (5) shows that E_B varies much less as a function of c/a than E_{Ew} since the valence electrons behave as an 'electron gas' and thus depend more on volume than on changes of the crystal structure. Consequently the stabilization energies are expected to be small, in contrast to those of transition metals, which will be discussed below.

3.8. Titanium and vanadium

Ti exhibits a complex phase diagram with an hcp ground state followed at 1155 K by the bcc structure which remains up to the melting temperature at 1943 K. Under pressure (and below 900 K) experiment finds a transition from hcp to the hexagonal ω-phase. A recent

Table 2. Calculated and experimental (in brackets) elastic data for Ca and Sr. A comparison with experiment is only possible for the low-temperature structure; experimental data are taken from [49]. The volume is given as volume per atom.

	B (GPa)	C' (GPa)	C_{11} (GPa)	C_{12} (GPa)	V_{equil} (bohr^3)
Ca fcc	19.2 (18.3)	2.9 (2.8)	23.1 (23.1)	17.2 (16.0)	256.9 (294.7)
Ca bcc	20.1	2.7	23.7	18.3	253.9
Sr fcc	16.5 (12.0)	1.8 (2.5)	18.9 (15.3)	15.3 (10.3)	324.0 (380.5)
Sr bcc	16.0	3.5	20.6	13.6	319.6

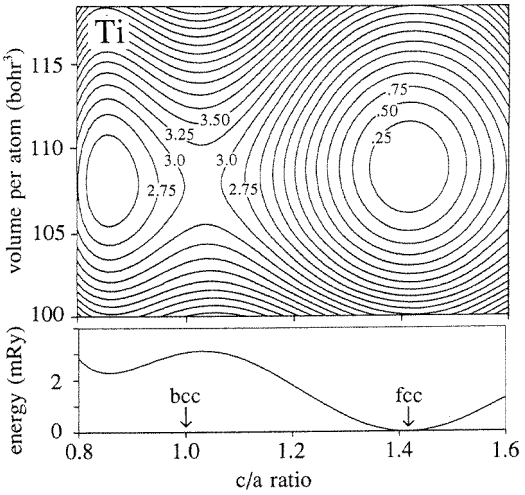

Figure 8. Total energy contours of Ti as a function of c/a and volume per atom. The energy difference between adjacent contour lines is 0.25 mRyd. The bottom panel shows a section of the energy surface at V_{equil}.

band structure investigation [43] predicts a further transition to the bcc structure at a pressure of 57 GPa. Ti does not exist in the fcc phase but since the hcp and the fcc structure are very similar (same nearest-neighbour coordination) we expect that the hcp phase is only slightly lower than the fcc modification. We find fcc already lower in energy than bcc (figure 8) but there is a qualitative difference from the simple metals, because the bcc modification ($c/a = 1$) now appears at a saddle point (a minimum with respect to V, but a maximum with respect to c/a). The energy difference between the fcc and the bcc state is about 3 mRyd which is considerably larger than for the simple metals discussed above. We find an additional metastable minimum at $c/a \approx 0.85$ apparent from the bottom panel of figure 8 which represents a section through the energy surface taken at V_{eq}. This peculiar behaviour requires an explanation, which is attempted below.

The ground state of vanadium (figure 9) is found to be bcc ($c/a = 1$) in agreement with experiment. The fcc phase corresponds to a saddle point at $c/a = \sqrt{2}$ at an energy about 20 mRyd above the bcc ground state followed by a metastable minimum at a large bct distortion (with $c/a = 1.8$). The section through the energy surface for constant volume V_{equil} (the bottom panel of figure 9) shows that the maximum (saddle point) and the minimum position are interchanged between V and Ti, but both appear at the cubic c/a values.

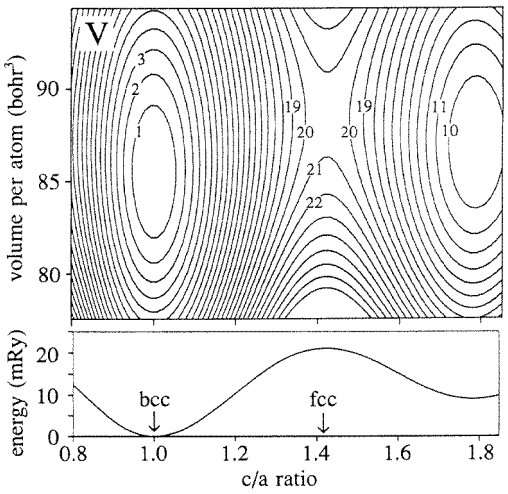

Figure 9. Total energy contours of V as a function of c/a and volume per atom. The energy difference between adjacent contour lines is 1.0 mRyd. The bottom panel shows a section of the energy surface at V_{equil}.

Both systems have the following characteristics in common that distinguish them from the simple metals. The equilibrium modification must and does lie in an absolute minimum of the total energy but there is always a second metastable minimum with a rather large tetragonal distortion at a c/a ratio of about 0.85 and 1.8, respectively. Although a similar behaviour has been found for the series of the 4d elements [14], as well as for bcc Fe [16], Co [44], and Mn [45] these features have not yet been explained and thus require an interpretation.

As discussed above (see the beginning of section 3) the total energy at constant volume contains two major contributions, namely the band energy E_B and the electrostatic Ewald energy E_{Ew}. In order to determine which of them dominates the structural stability, we show these two contributions in figure 10 (note the different energy scale for Ti and V). Let us first discuss V for which the band energy (circles) has a maximum at $c/a = \sqrt{2}$, while the electrostatic Ewald energy (triangles) shows a double-well structure with minima for bcc and fcc (cf figure 2). Adding the band energy to the Ewald energy yields the structural energy which agrees well with the FP LAPW total energy (full line) disregarding a constant energy shift. For V, both the structural and the total energy have an absolute minimum at $c/a = 1$, a maximum at $\sqrt{2}$, and a metastable minimum around 1.8. The latter minimum occurs since the electrostatic energy rises sharply for large c/a and thus dominates over the decreasing band energy.

Although the Ewald energy is similar for Ti and V, it is the band energy that makes the difference. An inspection of the cubic band structures reveals that the maximum in the band energy arises from the special position of the Fermi energy falling in a region of high density of states from nearly degenerate d bands, which are present in fcc V and to a lesser extent in bcc Ti but not in the other structure (bcc V or fcc Ti). A lifting of this degeneracy by the tetragonal distortion lowers the band energy for c/a above or below the respective cubic value causing the local maximum in the band energy. From this analysis we conclude that in d-electron systems the band energy is crucial in determining the structural energy and thus the c/a dependence. This is in contrast to the sp metals or to some ionic compounds

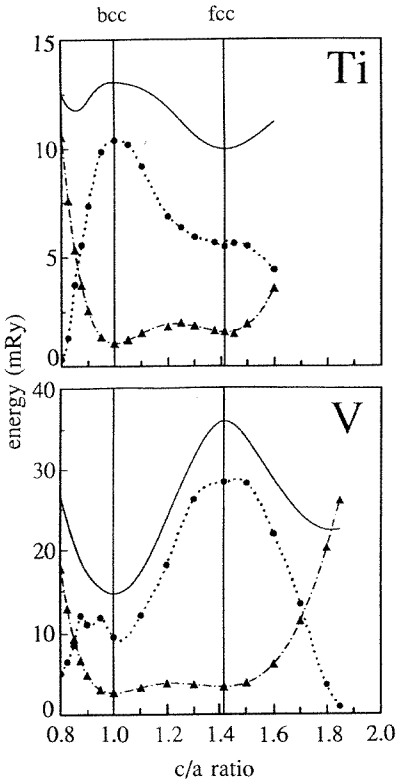

Figure 10. Contributions to the total energy (within an arbitrary energy shift) of Ti and V as a function of c/a: electrostatic (Ewald) energy (triangles, dashed–dotted curve), band energy (circles, dotted curve) and FP LAPW total energy (solid line). Note the different energy scale of the two systems.

(e.g. CsI), where the energy surface is largely determined by electrostatics.

This characteristic minimum/maximum behaviour, which occurs for the transition metals, allows us to relate the tetragonal shear constant C' to the energy difference ΔE taken between the saddle point and the equilibrium state. From a fit of the total energy in lowest order of c/a one obtains

$$C' \cong (1/V)6\Delta E/(\sqrt{2}-1)^2. \tag{7}$$

Employing (7) the values of C' calculated for Ti and V are 14.2 and 121 GPa, respectively; these compare well with the corresponding theoretical values due to (3) given in table 3, illustrating an internal consistency. This simple model also explains the correlation between ΔE and C' discussed in [14]. We note that (7) should not be applied to the simple metals since for them both the fcc and the bcc modification correspond to local minima in the total energy.

The largest discrepancy in the elastic properties (table 3) is found for C' of Ti. However, for this case we can only make a limited comparison, since experimental data are for hcp Ti while our study contains the related fcc structure. (Note that hcp Ti has a c/a ratio that is about 2.5% smaller than the ideal value.) The energy variation along the Bain path is large for V so C' cannot be obtained accurately enough from the polynomial fit (up to sixth order in c/a) but is obtained by direct numerical calculations for small c/a strains.

Table 3. Calculated and experimental (in brackets) elastic data for Ti and V, where experimental data are taken from [49] and volume is given per atom. For Ti the experiments correspond to the related hcp structure which is the true ground state.

	B (GPa)	C' (GPa)	C_{11} (GPa)	C_{12} (GPa)	V_{eq} (bohr^3)
Ti fcc	130 (113)	13.5 (35)	148 (160)	121 (90)	108.1 (119.3)
V bcc	220 (157)	76 (55)	288 (230)	136 (120)	84.81 (93.4)

4. Summary

The present investigation deals with the tetragonal distortion along the Bain path and provides a first step towards a better understanding of the energetics involved in phase transitions. These $T = 0$ K results are the basis for studying finite-temperature effects which will be discussed in part II of this paper [6].

Our calculations yield a qualitative difference in the total energy surfaces between the simple sp metals Li, K, Rb, Ca, and Sr and the transition metals Ti and V. For the simple metals the total energy as a function of the c/a ratio always has two minima at the 'cubic' values of c/a. For the transition metals we also find two minima but only one of them lies at a 'cubic' value of c/a whereas the second (metastable) minimum is found at either $c/a > \sqrt{2}$ (V) or $c/a < 1$ (Ti). The second respective 'cubic' value of c/a lies at a saddle point in the total energy surface (a minimum along V, but a maximum along c/a). This latter behaviour has also been found for bcc/fcc Fe [16] and for hcp/bcc Co [44] as well as for the intermetallic compounds TiAl, VAl, and CrAl [46]. This saddle point nature found in our calculations could be the reason for the experimentally observed limit in the thickness of epitaxially grown films [47, 48]. An interesting feature is the additional metastable minimum at larger tetragonal distortion found for Ti and V. This might challenge experimentalists to investigate whether this new structural modification can be stabilized. The equilibrium values for the elastic constants and volumes (tables 1–3) reproduce well the experimental trends. The remaining deviations between theory and experiment are due to the LDA, which systematically leads to about 10–15% too small a volume and correspondingly to a too large bulk modulus. For the transition metals we derive a simple relation between the stabilization energy and the shear constant C' which also explains the trends for the later transition metals [14].

Acknowledgment

One of us (VS) would like to thank the Austrian Science Foundation for the Lise–Meitner fellowship grant (FWF project number M0134-CHE). Some of the calculations were performed on the IBM RS-6000-550 provided by the Computer Centre at the University of Vienna.

Appendix

In tables A1–7 we supply the coefficients A_{ij} of the total energy surface as defined by (1). The coefficients in (1) are chosen such that on entering the volume per atom in bohr^3 the energy is obtained in Ryd/atom with respect to the lowest energy, which is set to zero. The caption of each table specifies the volume and c/a ranges for which the fit is valid. Within this range the accuracy of the fit is better than 10^{-5} Ryd.

The coefficients can also be obtained in electronically readable form. Please request via electronic mail: kschwarz@email.tuwien.ac.at.

Table A1. Lithium: $V_{max} = 136.0$, $V_{min} = 115.0$; $(c/a)_{max} = 1.6$, $(c/a)_{min} = 0.85$.

	$j = 0$	$j = 1$	$j = 2$	$j = 3$
$i = 0$	$0.158\,607\,12 \times 10^{2}$	$-0.367\,656\,15 \times 10^{0}$	$0.294\,039\,13 \times 10^{-2}$	$-0.790\,250\,03 \times 10^{-5}$
$i = 1$	$-0.805\,658\,88 \times 10^{2}$	$0.187\,414\,36 \times 10^{1}$	$-0.150\,128\,31 \times 10^{-1}$	$0.404\,303\,11 \times 10^{-4}$
$i = 2$	$-0.169\,677\,26 \times 10^{3}$	$-0.395\,751\,79 \times 10^{1}$	$0.317\,232\,49 \times 10^{-1}$	$-0.855\,173\,29 \times 10^{-4}$
$i = 3$	$-0.187\,650\,94 \times 10^{3}$	$0.439\,003\,14 \times 10^{1}$	$-0.352\,362\,33 \times 10^{-1}$	$0.951\,301\,72 \times 10^{-4}$
$i = 4$	$0.114\,964\,54 \times 10^{3}$	$-0.269\,857\,50 \times 10^{1}$	$0.217\,000\,68 \times 10^{-1}$	$-0.587\,001\,19 \times 10^{-4}$
$i = 5$	$-0.370\,138\,74 \times 10^{2}$	$0.871\,937\,75 \times 10^{0}$	$-0.702\,779\,01 \times 10^{-2}$	$0.190\,553\,59 \times 10^{-4}$
$i = 6$	$0.489\,607\,62 \times 10^{1}$	$-0.115\,765\,69 \times 10^{0}$	$0.935\,601\,85 \times 10^{-3}$	$-0.254\,366\,01 \times 10^{-5}$

Table A2. Potassium: $V_{max} = 500.0$, $V_{min} = 300.0$; $(c/a)_{max} = 1.5$, $(c/a)_{min} = 0.90$.

	$j = 0$	$j = 1$	$j = 2$	$j = 3$
$i = 0$	$0.554\,022\,25 \times 10^{0}$	$-0.320\,808\,51 \times 10^{-2}$	$0.100\,285\,27 \times 10^{-4}$	$-0.103\,281\,96 \times 10-7$
$i = 1$	$-0.329\,580\,23 \times 10^{1}$	$0.222\,082\,74 \times 10^{-1}$	$-0.646\,936\,38 \times 10^{-4}$	$0.616\,164\,25 \times 10^{-7}$
$i = 2$	$0.867\,303\,22 \times 10^{1}$	$-0.612\,404\,93 \times 10^{-1}$	$0.164\,963\,30 \times 10^{-3}$	$-0.145\,899\,79 \times 10^{-6}$
$i = 3$	$-0.984\,329\,09 \times 10^{1}$	$0.709\,229\,79 \times 10^{-1}$	$-0.184\,139\,82 \times 10^{-3}$	$0.156\,690\,01 \times 10^{-6}$
$i = 4$	$0.512\,897\,29 \times 10^{1}$	$-0.373\,515\,84 \times 10^{-1}$	$0.949\,246\,05 \times 10^{-4}$	$-0.788\,975\,23 \times 10^{-7}$
$i = 5$	$-0.100\,921\,07 \times 10^{1}$	$0.739\,574\,55 \times 10^{-2}$	$-0.185\,339\,11 \times 10^{-4}$	$0.151\,642\,52 \times 10^{-7}$

Table A3. Rubidium: $V_{max} = 570.0$, $V_{min} = 440.0$; $(c/a)_{max} = 1.5$, $(c/a)_{min} = 0.90$.

	$j = 0$	$j = 1$	$j = 2$	$j = 3$
$i = 0$	$0.134\,511\,40 \times 10^{2}$	$-0.912\,663\,10 \times 10^{-1}$	$0.207\,507\,95 \times 10^{-3}$	$-0.155\,045\,50 \times 10^{-6}$
$i = 1$	$-0.595\,870\,52 \times 10^{2}$	$0.405\,089\,25 \times 10^{0}$	$-0.920\,038\,70 \times 10^{-3}$	$0.686\,087\,58 \times 10^{-6}$
$i = 2$	$0.106\,108\,28 \times 10^{3}$	$-0.720\,003\,94 \times 10^{0}$	$0.162\,890\,54 \times 10^{-2}$	$-0.120\,985\,16 \times 10^{-5}$
$i = 3$	$-0.934\,172\,47 \times 10^{2}$	$0.632\,702\,81 \times 10^{0}$	$-0.142\,626\,32 \times 10^{-2}$	$0.105\,532\,44 \times 10^{-5}$
$i = 4$	$0.406\,670\,95 \times 10^{2}$	$-0.274\,908\,74 \times 10^{0}$	$0.617\,418\,32 \times 10^{-3}$	$-0.455\,354\,67 \times 10^{-6}$
$i = 5$	$-0.700\,191\,96 \times 10^{1}$	$0.472\,435\,23 \times 10^{-1}$	$-0.105\,776\,53 \times 10^{-3}$	$0.777\,467\,18 \times 10^{-7}$

Table A4. Calcium: $V_{max} = 270.0$, $V_{min} = 235.0$; $(c/a)_{max} = 1.6$, $(c/a)_{min} = 0.80$.

	$j = 0$	$j = 1$	$j = 2$	$j = 3$
$i = 0$	$0.137\,168\,68 \times 10^{3}$	$-0.168\,633\,04 \times 10^{2}$	$0.688\,156\,54 \times 10^{-1}$	$-0.930\,928\,18 \times 10^{-4}$
$i = 1$	$-0.767\,978\,44 \times 10^{4}$	$0.943\,590\,09 \times 10^{2}$	$-0.384\,838\,96 \times 10^{0}$	$0.520\,414\,83 \times 10^{-3}$
$i = 2$	$0.176\,464\,40 \times 10^{5}$	$-0.216\,675\,12 \times 10^{3}$	$0.883\,169\,50 \times 10^{0}$	$-0.119\,383\,69 \times 10^{-2}$
$i = 3$	$-0.212\,910\,78 \times 10^{5}$	$0.261\,258\,95 \times 10^{3}$	$-0.106\,428\,74 \times 10^{1}$	$0.143\,813\,54 \times 10^{-2}$
$i = 4$	$0.142\,260\,99 \times 10^{5}$	$-0.174\,458\,71 \times 10^{3}$	$0.710\,313\,52 \times 10^{0}$	$-0.959\,493\,48 \times 10^{-3}$
$i = 5$	$-0.499\,239\,46 \times 10^{4}$	$0.611\,877\,46 \times 10^{2}$	$-0.249\,005\,63 \times 10^{0}$	$0.336\,250\,68 \times 10^{-3}$
$i = 6$	$0.719\,213\,89 \times 10^{3}$	$-0.881\,006\,28 \times 10^{1}$	$0.358\,366\,94 \times 10^{-1}$	$-0.483\,786\,61 \times 10^{-4}$

Table A5. Strontium: $V_{max} = 380.0$, $V_{min} = 290.0$; $(c/a)_{max} = 1.6$, $(c/a)_{min} = 0.80$.

	$j = 0$	$j = 1$	$j = 2$	$j = 3$
$i = 0$	$-0.373\,654\,20 \times 10^{2}$	$0.315\,475\,46 \times 10^{0}$	$-0.873\,363\,72 \times 10^{-3}$	$0.806\,663\,87 \times 10^{-6}$
$i = 1$	$0.179\,236\,16 \times 10^{3}$	$-0.149\,903\,94 \times 10^{1}$	$0.413\,924\,28 \times 10^{-2}$	$-0.382\,675\,34 \times 10^{-5}$
$i = 2$	$-0.342\,752\,67 \times 10^{3}$	$0.283\,866\,73 \times 10^{1}$	$-0.781\,543\,05 \times 10^{-2}$	$0.723\,313\,78 \times 10^{-5}$
$i = 3$	$0.337\,114\,42 \times 10^{3}$	$-0.276\,053\,85 \times 10^{1}$	$0.756\,904\,12 \times 10^{-2}$	$-0.700\,715\,72 \times 10^{-5}$
$i = 4$	$-0.178\,970\,88 \times 10^{3}$	$0.144\,500\,76 \times 10^{1}$	$-0.393\,818\,96 \times 10^{-2}$	$0.364\,318\,30 \times 10^{-5}$
$i = 5$	$0.482\,572\,75 \times 10^{2}$	$-0.382\,200\,59 \times 10^{0}$	$0.103\,188\,78 \times 10^{-2}$	$-0.952\,335\,87 \times 10^{-6}$
$i = 6$	$-0.509\,023\,07 \times 10^{1}$	$0.391\,478\,57 \times 10^{-1}$	$-0.103\,997\,86 \times 10^{-3}$	$0.954\,486\,66 \times 10^{-7}$

Table A6. Titanium: $V_{max} = 117.0$, $V_{min} = 100.0$; $(c/a)_{max} = 1.6$, $(c/a)_{min} = 0.80$.

	$j = 0$	$j = 1$	$j = 2$	$j = 3$
$i = 0$	$0.942\,944\,28 \times 10^{3}$	$-0.250\,452\,46 \times 10^{2}$	$0.219\,807\,90 \times 10^{0}$	$-0.634\,972\,40 \times 10^{-3}$
$i = 1$	$-0.496\,833\,58 \times 10^{4}$	$0.131\,954\,28 \times 10^{3}$	$-0.115\,783\,34 \times 10^{1}$	$0.334\,409\,60 \times 10^{-2}$
$i = 2$	$0.108\,471\,57 \times 10^{5}$	$-0.288\,078\,78 \times 10^{3}$	$0.252\,737\,58 \times 10^{1}$	$-0.729\,945\,94 \times 10^{-2}$
$i = 3$	$-0.125\,413\,68 \times 10^{5}$	$0.333\,092\,73 \times 10^{3}$	$-0.292\,229\,96 \times 10^{1}$	$0.844\,173\,56 \times 10^{-2}$
$i = 4$	$0.809\,428\,90 \times 10^{4}$	$-0.215\,005\,92 \times 10^{3}$	$0.188\,650\,52 \times 10^{1}$	$-0.545\,157\,19 \times 10^{-2}$
$i = 5$	$-0.276\,328\,06 \times 10^{4}$	$0.734\,112\,03 \times 10^{2}$	$-0.644\,242\,01 \times 10^{0}$	$0.186\,258\,82 \times 10^{-2}$
$i = 6$	$0.389\,628\,43 \times 10^{3}$	$-0.103\,528\,28 \times 10^{2}$	$0.908\,748\,19 \times 10^{-1}$	$-0.262\,869\,88 \times 10^{-3}$

Table A7. Vanadium: $V_{max} = 93.0$, $V_{min} = 77.5$; $(c/a)_{max} = 1.85$, $(c/a)_{min} = 0.80$.

	$j = 0$	$j = 1$	$j = 2$	$j = 3$
$i = 0$	$0.615\,549\,76 \times 10^{3}$	$-0.223\,171\,17 \times 10^{2}$	$0.264\,583\,30 \times 10^{0}$	$-0.103\,608\,53 \times 10^{-2}$
$i = 1$	$-0.287\,094\,26 \times 10^{4}$	$0.104\,393\,54 \times 10^{3}$	$-0.123\,897\,12 \times 10^{1}$	$0.485\,324\,19 \times 10^{-2}$
$i = 2$	$0.550\,389\,54 \times 10^{4}$	$-0.200\,514\,52 \times 10^{3}$	$0.238\,071\,11 \times 10^{1}$	$-0.932\,363\,56 \times 10^{-2}$
$i = 3$	$-0.553\,984\,81 \times 10^{4}$	$0.202\,064\,78 \times 10^{3}$	$-0.239\,922\,51 \times 10^{1}$	$0.939\,210\,62 \times 10^{-2}$
$i = 4$	$0.309\,046\,69 \times 10^{4}$	$-0.112\,771\,29 \times 10^{3}$	$0.133\,854\,35 \times 10^{1}$	$-0.523\,643\,60 \times 10^{-2}$
$i = 5$	$-0.906\,803\,20 \times 10^{3}$	$0.330\,781\,47 \times 10^{2}$	$-0.392\,342\,02 \times 10^{0}$	$0.153\,347\,60 \times 10^{-2}$
$i = 6$	$0.109\,424\,92 \times 10^{3}$	$-0.398\,747\,06 \times 10^{1}$	$0.472\,451\,49 \times 10^{-1}$	$-0.184\,450\,28 \times 10^{-3}$

References

[1] Cochran W 1960 *Adv. Phys.* **9** 387
[2] Anderson P W 1960 *Fizika Dielectrikov* ed G I Skanavi (Moscow: Akad. Nauk SSR)
[3] Clapp P C 1973 *Phys. Status Solidi* b **57** 561
[4] Krumhansl J A 1992 *Solid State Commun.* **48** 251
[5] Krumhansl J A and Gooding R J 1989 *Phys. Rev.* B **39** 3047
[6] Mohn P, Schwarz K and Blaha P 1995 *J. Phys.: Condens. Matter* at press
[7] Vul D A and Harmon B N 1993 *Phys. Rev.* B **48** 6880
[8] Olson G B and Owen W S (ed) 1992 *Martensite* (ASM International)
[9] Bain E C 1924 *Trans. AIME* **70** 25
[10] Ye Y Y, Chan C T, Ho K M and Harmon B N 1990 *Int. J. Supercomput. Appl.* **4** 111
[11] Sigalas M, Bacalis N C, Papaconstantopoulos D A, Mehl M J and Switendick A C 1990 *Phys. Rev.* B **42** 11 637
[12] Blaha P, Schwarz K, Dufek P and Augustyn R 1995 *Computer Code WIEN95* (Vienna: Technical University of Vienna) (an improved and updated Unix version of the original copyrighted WIEN code, Blaha P, Schwarz K, Sorantin P and Trickey S B 1990 *Comput. Phys. Commun.* **59** 399)
[13] Hedin L and Lundqvist S 1971 *J. Phys.: Condens. Matter* **4** 2064

[14] Wills J M, Eriksson O, Söderlind P and Boring A M 1992 *Phys. Rev. Lett.* **68** 2802
[15] Chen Y, Ho K M and Harmon B N 1988 *Phys. Rev.* B **37** 283
[16] Krasko G L and Olson G B 1989 *Phys. Rev.* B **40** 11 536
[17] Wentzcovich R M and Krakauer H 1990 *Phys. Rev.* B **42** 4563
[18] Khachaturyan A G 1983 *Theory of Structural Transformation in Solids* (New York: Wiley)
[19] Weinert M, Wimmer E and Freeman A J 1982 *Phys. Rev.* B **26** 4571
[20] Heine V and Weaire D 1970 *Solid State Physics* vol 24 ed H Ehrenreich, F Seitz and D Turnbull (New York: Academic) p 247
[21] Christensen N E and Satpathy 1985 *Phys. Rev. Lett.* **55** 600
[22] Young D A 1991 *Phase Diagrams of the Elements* (Berkeley, Los Angeles, Oxford: University of California Press)
[23] Berliner R, Fajen O, Smith H G and Hitterman R L 1989 *Phys. Rev.* B **40** 12 086
[24] Nobel J A, Trickey S B, Blaha P and Schwarz K 1992 *Phys. Rev.* **45** 5012
[25] Vaks V G, Katsnelson M I, Koreshkov V G, Lichtenstein A I, Parfenov O E, Skok V F, Sukhoparov V A, Trefilov A V and Chernyshov A A 1989 *J. Phys.: Condens. Matter* **1** 5319
[26] Skriver H L 1985 *Phys. Rev.* B **31** 1909
[27] Perdew J P, Chevary J A, Vosko S H, Jackson K A, Pederson M R, Singh D H and Fiolhais C 1992 *Phys. Rev.* B **46** 6671
[28] Dacorogna M M and Cohen M L 1986 *Phys. Rev.* B **34** 4996
[29] McMahan A K and Moriarty J A 1983 *Phys. Rev.* B **27** 3235
[30] Papaconstantopoulos D A and Singh D J 1992 *Phys. Rev.* B **45** 7507
[31] Alouani M, Christensen N E and Syassen K 1989 *Phys. Rev.* B **39** 8096
[32] Giebultowicz T M, Overhauser A W and Werner S A 1986 *Phys. Rev. Lett.* **56** 1485
[33] Blaschko O, de Podesta M and Pintschovius L 1988 *Phys. Rev.* B **37** 4258
[34] Templeton I M 1982 *J. Phys. F: Met. Phys.* **12** L121
[35] Maysenhölder W, Louie S G and Cohen M L 1985 *Phys. Rev.* B **31** 1817
[36] Gooding R J, Ye Y Y, Chan C T, Ho K M and Harmon B N 1991 *Phys. Rev.* B **43** 13 626
[37] Grimvall G and Ebbsjö I 1975 *Phys. Scr.* **12** 168
Grimvall G 1975 *Phys. Scr.* **12** 173
[38] Jones H 1960 *The Theory of Brillouin Zones and Electronic States in Crystals* (Amsterdam: North-Holland)
[39] Olijnyk H and Holzapfel W B 1984 *Phys. Lett.* **100** 191
[40] Burgers W G 1935 *Physica* **1** 561
[41] Singh D 1991 *Phys. Rev.* B **43** 6388
[42] Skriver H L 1982 *Phys. Rev. Lett.* **49** 1768
[43] Ahuja R, Wills J M, Johansson B and Eriksson O 1993 *Phys. Rev.* B **48** 16 269
[44] Liu A Y and Singh D S 1993 *Phys. Rev.* B **47** 8515
[45] Sliwko V L unpublished results
[46] Zou J and Fou C L 1995 *Phys. Rev.* B **51** 2115
[47] Prinz G A 1985 *Phys. Rev. Lett.* **54** 1051
[48] Liu C and Bader S D 1989 *Physica* B **161** 253
[49] 1991 *Landolt–Börnstein New Series* vol 111/29a ed D F Nelson (Heidelberg: Springer)